JCTC Journal of Chemical Theory and Computation

Molecular Polarization Effects on the Relative Energies of the Real and Putative Crystal Structures of Valine

Timothy G. Cooper, Katarzyna E. Hejczyk, William Jones, and Graeme M. Day*

The Pfizer Institute for Pharmaceutical Materials Science, Department of Chemistry, University of Cambridge, Lensfield Road, Cambridge CB2 1EW, United Kingdom

Received May 28, 2008

Abstract: The computer-generation of the crystal structures of the α-amino acid valine is used as a challenging test of lattice energy modeling methods for crystal structure prediction of flexible polar organic molecules and, specifically, to examine the importance of molecular polarization on calculated relative energies. Total calculated crystal energies, which combine atom-atom model potential calculations of intermolecular interactions with density functional theory intramolecular energies, do not effectively distinguish the real (known) crystal structures from the rest of the low energy computer-generated alternatives when the molecular electrostatic models are derived from isolated molecule calculations. However, we find that introducing a simple model for the bulk crystalline environment when calculating the molecular energy and electron density distribution leads to important changes in relative total crystal energies and correctly distinguishes the observed crystal structures from the set of computer-generated possibilities. This study highlights the importance of polarization of the molecular charge distribution in crystal structure prediction calculations, especially for polar flexible molecules, and suggests a computationally inexpensive approach to include its effect in lattice energy calculations.

Introduction

The identification or prediction of the most stable crystalline form of an organic molecule is of considerable scientific interest but remains a challenge for both experimental and computational methods. In particular, to avoid any unanticipated polymorphic change during manufacturing it is vitally important in the pharmaceutical industry to know that the crystalline form being produced is the thermodynamically most stable. Such a change in form could have unpredictable effects on processing and tabletting of the drug as well as its final bioavailability, since polymorphs can have markedly different dissolution rates.[1] For this reason, great amounts of time and money are spent screening for polymorphs to maximize the likelihood that all crystal forms of the drug molecule have been found.[2] If theoretical studies could identify all possible crystal structures of a particular organic molecule and reliably predict their relative thermodynamic stabilities, such calculations could help inform and possibly direct the current experimental approaches used to produce the different crystal forms.

A variety of computational methods have been developed for crystal structure prediction (CSP), with the aim of producing the possible crystal structures of a particular molecule using only the chemical formula as input.[3] The difficulty in CSP is not necessarily in generating all crystal packing possibilities, including the observed crystal structure (or structures, where the molecule displays polymorphism), but in identifying those structures that will be experimentally observed from the many putative structures; often there are tens or even hundreds of distinct crystal structures (local minima on the lattice energy surface) within a small (e.g., 5 kJ mol^{-1}) range in lattice energy,[4] and the assumption is that the lowest energy structure is the most likely structure to be observed experimentally. CSP of rigid organic molecules is well developed, and, using a sufficiently high quality model intermolecular potential, the observed crystal structure(s) are quite reliably found among a small set of the lowest energy computationally generated structures.[5] How-

* Corresponding author e-mail: gmd27@cam.ac.uk.

10.1021/ct800195g CCC: $40.75
Published on Web 09/11/2008

ever, predicting the crystal structures of molecules with conformation freedom is an entirely more difficult proposition. There are two causes of difficulties associated with molecular flexibility: a) the conformational search space that needs to be sampled when searching for all crystal packing possibilities, with each degree of intramolecular freedom adding an extra dimension to the already large and complex search space, and b) comparison of the energies of putative crystal structures, which involves calculation of a lattice (*inter*molecular) and a conformational (*intra*molecular) component for the generated crystal structures, with the two components needing to be both accurate and balanced with respect to each other.

We have chosen the series of α-amino acid crystal structures as a test set for the development of CSP methods for conformationally flexible molecules. This family of molecules was chosen for several reasons: their biological importance; the importance of amino acid functional groups in pharmaceutical molecules; and because the series of similar molecules allows stepwise progression from systems with very limited molecular flexibility to larger, more flexible molecules. The striking differences in conformations between the gas phase and the solid state make amino acids very challenging systems to study, especially using the most common approach to CSP, where molecular geometries are derived from isolated molecule calculations. A study by Görbitz[6] of the chiral hydrophobic α-amino acids, using hydrogen bonding donor and acceptor sites to simulate the surrounding crystal, has shown that the conformations found in the crystals can be reproduced by quantum mechanics methods. However, there is flexibility about both the carboxylate and amino groups in the α amino acids, and the observed conformations in crystal structures vary considerably, e.g. the $H_\alpha-C_\alpha-C-O$ dihedral angle in the four published polymorphs of glycine in the Cambridge Structural Database[7] (CSD) varies between 35° and 84°.

One approach to CSP for moderately flexible molecules is to consider a set of fixed molecular geometries, normally obtained from quantum mechanical (QM) calculations *via* a scan of the flexible intramolecular degrees of freedom. Alternatively, conformations can be chosen by comparison to known crystal structures of similar molecules. In both approaches, crystal structures are generated with each conformation, and the total energies used to evaluate the relative stabilities of the resulting crystal structures are calculated as

$$U_{total} = \sum_{i\in M, k\in N} [A_{\iota\kappa}\exp(-B_{\iota\kappa}R_{ik}) - C_{\iota\kappa}R_{ik}^{-6} + U_{electrostatic}(\rho_M, \rho_N)] + U_{molecular}(\mathrm{QM}, \rho) \quad (1)$$

where the terms in the summation represent intermolecular interactions in the crystal, and $U_{molecular}$ is the energy of the molecular conformation in that crystal structure. Here, $U_{molecular}$ is taken from the QM evaluation of the molecular energy. $A_{\iota\kappa}$, $B_{\iota\kappa}$, and $C_{\iota\kappa}$ are empirically derived parameters describing the repulsion-dispersion interactions between atoms i and k in molecules M and N; ι and κ are the atom types of atoms i and k, respectively. $U_{electrostatic}$ is calculated from a representation of the molecular charge density, ρ, either by a set of partial charges distributed around the molecule (typically at atomic positions) or by a multipole expansion (i.e., charge, dipole, quadrupole, etc.) at each atomic site.

In preliminary studies of the crystal packings of valine and other flexible molecules, we have observed that the above approach, combining atomistic (*inter*molecular) with quantum mechanical (*intra*molecular) energies, resulted in an imbalance between the *inter*- and *intra*molecular contributions to the relative energies of putative crystal structures. In particular, the intramolecular energies were often found to dominate the ranking of structures, and, while the true crystal structures stand out as having among the best intermolecular energies, those with the lowest *total* energies all had favorable *intra*molecular energies but poor *inter*molecular energies. The energy model is dominated by the QM calculated conformational energy. We therefore sought to correct the imbalance between the two energy contributions in the computational method, which we propose is largely due to molecular polarization being ignored in the intermolecular model, i.e. the electrostatic interactions in eq 1 are based on the charge density (ρ) of the isolated molecule.

Deriving the electrostatic model from isolated molecule charge densities ignores the rearrangement of the molecular electron density due to the crystalline environment, which is known to be important in molecular crystals.[8] This polarization serves to lower the total crystal energy by strengthening the intermolecular interactions between molecular electron densities. Therefore, models derived from isolated molecule (i.e., nonpolarized) charge densities will underestimate intermolecular electrostatic stabilization energies, which are dominant for systems with significant charge separation, such as salts or zwitterionic molecules (such as the α-amino acids). One strategy used to model induction effects is to include molecular or atomic polarizabilities in the atom-atom model, as is done in polarizable force fields.[9,10] The theory for calculating the resulting induction energy has been presented elsewhere,[11,12] and methods are continually developing for the derivation of such atomic polarizabilities.[13,14] An alternative is to perform the molecular charge density calculation in an environment representative of the crystal, so that the atomic partial charge or multipole analysis is performed on a molecular electron density that is a better representation of the molecule in the crystal. The two approaches have recently been compared in an investigation of the magnitude of induction energy contributions to the energies of molecular organic crystal structures.[15] We have followed the latter approach here and investigate the influence of a very simple description of the bulk crystal environment during the molecular QM calculation: the environment of the molecule in the crystal is modeled as a polarizable continuum, in the same way that solvation effects on molecular properties are often modeled, using Tomasi and co-workers' polarizable continuum model (PCM)[16−18] with dielectric constants typical of molecular organic crystals.

We test this approach for valine, the α-amino acid with an isopropyl side group, and, as such, one more flexible torsion angle than alanine, whose crystal structures we

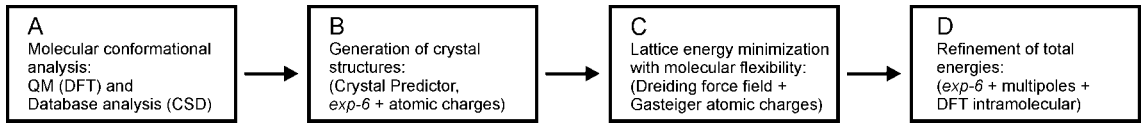

Figure 1. Outline of the crystal structure prediction methodology applied here to valine.

studied previously.[19] The two known racemic polymorphs (monoclinic,[20] CSD refcode VALIDL and triclinic[21] VALIDL02, both with $Z' = 1$) have almost identical molecular conformations and crystal packings and only differ by the relative orientation of pairs of hydrogen bonded layers. Enantiopure valine crystallizes with two molecules in the asymmetric unit[22] ($Z' = 2$, refcode LVALIN01) and, while we have not performed the computationally expensive task of generating and energy minimizing all possible $Z' = 2$ structures, we compare the calculated energy of the known structure with the computer-generated $Z' = 1$ alternative crystal structures to confirm that the observed $Z' = 2$ form is lower in energy than the $Z' = 1$ possibilities.

Methods

Overall Approach. We combine our general strategy for treating molecular flexibility in CSP[23] with database guided sampling of conformational space,[19] which is necessary because of the extreme differences in molecular structure between the gas and crystalline phases for the α-amino acids.

The procedure comprises 4 steps (Figure 1):

A) analysis of the molecular conformations using both QM electronic structure calculations and crystal structures of similar molecules from the CSD; (B) generation of possible crystal packings with rigid molecular conformations from (A) *via* a sampling of unit cell parameters, molecular positions, and molecular orientations, within the most likely space groups; C) energy minimization of the computer-generated crystal structures with a molecular mechanics description of angle bending and torsion angles, allowing selected intramolecular degrees of freedom to adjust to the crystal environment, and D) final energy refinement using an accurate description of intermolecular interactions, in particular using a detailed description of the molecular electrostatic distribution.

The emphasis of the current study is on the final step in the procedure, where we aim to develop methods for evaluating the relative energies of the computer-generated crystal structures as accurately as possible, bearing in mind the associated computational expense and the need for methods of evaluating thousands of crystal structures in a reasonable time. As a result of the strong electrostatic interactions in the crystal structures of zwitterionic molecules, we chose this system to test a simple method of accounting for polarization effects on the calculated relative energies.

Molecular Conformational Analysis. We treated valine as having three flexible torsion angles (Figure 2), assuming that the methyl group orientations are unimportant to the crystal packing. For geometry optimizations and the torsion angle scan of the isopropyl group (Step A), we performed density functional theory (VWN/DNP) calculations on the isolated molecule using the Dmol3 module[24] within the

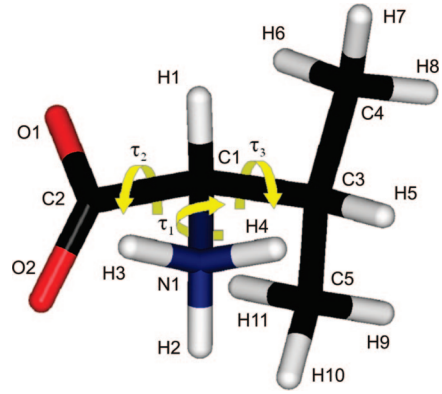

Figure 2. Molecular model of valine showing the definition of the three flexible torsion angles ($\tau_1 = H_2-N_1-C_1-H_1$, $\tau_2 = O_1-C_2-C_1-H_1$, $\tau_3 = H_5-C_3-C_1-H_1$). The amino torsion angle (τ_1) is shown in the staggered conformation.

Accelrys Materials Studio package.[25] Full geometry optimization of the valine molecule leads to the nonzwitterionic form, so it was necessary to constrain the three N−H bond lengths to maintain the zwitterionic form; we used a N−H bond length of 1.035 Å, the mean value from neutron diffraction α-amino acid crystal structures in the CSD. The isopropyl group of valine was scanned for the full range of torsion angles ($0° \le \tau_3 \le 360°$) in 20° intervals, with the angle measured between the α-hydrogen atom and the β-hydrogen atom of the isopropyl group ($\tau_3 = H-C-C-H$, Figure 2). The amino group was kept fixed in the staggered conformation ($\tau_1 = H-N-C-H = 180°$), while all other degrees of freedom were allowed to relax at each point in the scan.

Generation of Crystal Structures. We generated trial crystal structures (Step B) using the Crystal Predictor code, which employs a low-discrepancy sequence to search the crystal packing space with quasi-random values for unit cell parameters, molecular orientations, and positions followed by rigid molecule lattice energy minimization.[26] Searches were performed with a set of 15 rigid molecular geometries (see Results and Discussion), chosen in a similar way to our crystal packing study of alanine,[19] to sample the relevant region of the conformational energy surface. Crystal structures were generated in 12 space groups: the 5 most commonly observed chiral space groups for organic molecular crystals ($P2_12_12_1$, $P2_1$, $P1$, $P2_12_12$, and $C2$) and the 7 most common space groups with mirror or inversion symmetry ($P2_1/c$, $Pna2_1$, $Pnma$, $C2/c$, $P\bar{1}$, $Pbca$, and $Pbcn$). These account for over 90% of all the entries found in chiral and racemic space groups in the CSD.[27] Searches were continued until 50000 lattice energy minimizations had been performed for each conformation. We monitored convergence of the set of low energy structures, and 50000 minimizations were sufficient to give an apparently complete sampling in all cases. We then merged the set of predicted crystal structures

from each molecular conformation (keeping racemic and chiral crystal structures separate), and the structures were clustered to remove duplicates (the clustering algorithm is described below).

Model Potentials. For lattice energy minimizations during the initial crystal structure search (step B), we used an *exp-6* model potential with Williams and co-workers' empirically derived parameters to describe C, N, O, and H_C (hydrogen bonded to carbon)[28,29] and polar hydrogen atom (H_N) parameters taken from Coombes et al.[30] Electrostatic interactions were modeled by molecular electrostatic potential (ESP) fitted atomic partial charges obtained from a single point DFT calculation of the gas phase molecule (DMol3, VWN/DNP). For the final energy minimizations (Figure 1, step D), we applied the same *exp-6* model potential but with a more elaborate description of electrostatic interactions, using a distributed multipole model. Atomic multipoles, $Q^i{}_u$, up to hexadecapole on each atom i (the subscript u refers to the multipole component), were taken from a distributed multipole analysis (DMA) of a B3LYP/6−31G** electron density, calculated for the specific molecular conformation under consideration using the Gaussian03 program.[31] The DMA was performed using the program GDMA,[32] using the original DMA algorithm.[33,34] Final lattice energy minimizations were performed using the DMAREL crystal structure modeling program.[35] All *exp-6* interactions were evaluated up to a 15 Å cutoff, Ewald summation was employed for charge−charge, charge−dipole, and dipole−dipole electrostatic interactions, and all higher order electrostatic interactions (up to R^{-5}) were summed to a 15 Å cutoff on whole molecules.

Crystal structures were also lattice energy minimized using the same *exp-6* model potential with distributed multipoles derived from polarized molecular electron densities. These polarized electron densities were calculated using the polarizable continuum model (PCM),[16−18] as implemented in Gaussian03, to model the environment of the molecule. The united atom topological model (UA0) was used for atomic radii, with several choices of dielectric constant (ranging from $\epsilon = 3$ to 11). As with the unpolarized electrostatic model, the GDMA program was used to perform the distributed multipole analysis of the resulting charge density, and lattice energy minimizations were performed within the program DMAREL. The resulting atomic multipoles (from the PCM molecular calculations) differ from the unpolarized multipoles (the isolated molecule) by $\Delta Q^i{}_u$, and the resulting induction energy is a sum of two terms: the amplified intermolecular electrostatic interactions and the partly counteracting increase in internal molecular energy (ΔU_{mol}) upon distortion of the molecular charge distribution. In the purely classical approach, a classical expression is used for the internal molecular energy contribution (i.e., assuming that the molecular energy increases bilinearly with the ΔQ: $\Delta U_{mol} = {}^1/_2 \sum_{u,u',i,i'} \Delta Q^i{}_u \xi^{ii'}{}_{uu'} \Delta Q^{i'}{}_{u'}$).[11,12] The resulting expression for the induction energy requires the interaction of $\Delta Q^i{}_u$ on a reference molecule with $Q^i{}_u$ on all surrounding molecules. Using standard lattice energy modeling software, where all molecules possess the same set of atomic multipoles, two calculations are required to obtain this energy: one where all molecules are assigned atomic multipoles ($Q^i{}_u + \Delta Q^i{}_u/2$) and a second where all molecules have atomic multipoles ($\Delta Q^i{}_u/2$).[15] However, as we perform a molecular QM calculation for each crystal structure in this work, we can avoid the classical approximation to ΔU_{mol}. Instead, we take the increase in molecular energy directly from the density functional theory calculations on the isolated molecule and the molecule in the PCM environment, e.g. at $\epsilon = 3$ we take $\Delta U_{mol} = U_{mol}[\text{DFT}, \rho(\epsilon{=}3)] - U_{mol}[\text{DFT}, \rho(\text{vacuum})]$, where the interaction energy between the molecule and the dielectric continuum is excluded from $U_{mol}[\text{DFT}, \rho(\epsilon{=}3)]$. We then use the total polarized atomic multipoles ($Q^i{}_u + \Delta Q^i{}_u$) in our intermolecular energy calculations, which give the sum of electrostatic and the intermolecular part of the induction energy.

The final total crystal energies (in step D) were calculated as the sum of inter- and intramolecular energy terms, the *inter*molecular contribution taken from the *exp-6* + DMA model, and the *intra*molecular contribution from the DFT molecular energy calculation. The magnitude of the induction energy can be evaluated from the difference in the calculated intermolecular electrostatic energies from the ρ(PCM,ϵ) and ρ(vacuum) models + ΔU_{mol}:

$$U_{induction}(\varepsilon) = (U_{electr}[\rho(\varepsilon)] - U_{electr}[\rho(\text{vacuum})]) + (U_{mol}[\text{DFT},\rho(\varepsilon)] - U_{mol}[\text{DFT},\rho(\text{vacuum})]) \quad (2)$$

Flexible Force Fields. We tested four flexible molecule force fields (CVFF,[36] COMPASS,[37] Dreiding,[38] and UFF[39]) for the intermediate lattice energy calculation where molecular flexibility is allowed (Step C). The purpose of this step in the procedure is to allow the molecular geometry, which was held rigid during the initial generation of trial crystal structures, to adjust to its crystal environment. Force field partial charges were used for the CVFF and COMPASS force fields, while Gasteiger partial charges[40] were used with UFF and the Dreiding force field. Using a similar method in our study of phenobarbital crystal structures,[23] the computer-generated crystal structures were energy minimized with the molecules treated as comprising four rigid units: the amine (NH_3), carboxylate (CO_2), and isopropyl (C_3H_7) groups and the central CH to which they are all bonded, with reorientation of rigid units allowed relative to one another using the force field energy terms for the conformational energy. The internal structure of the rigid units was constrained at the DFT optimized geometries.

Comparison and Clustering of Structures. To compare the predicted and observed crystal structures and for removal of duplicate crystal structures ("clustering"), we used the Compack algorithm[41] with a tolerance of 20% on interatomic distances (excluding hydrogen atoms) within a cluster of 15 molecules (i.e., a central molecule and a coordination sphere of its 14 nearest neighbors). Clustering was used to remove duplicate crystal structures between steps B and C (Figure 1) and after the final energy minimizations in step D. After step B some crystal packings are found in searches using more than one molecular model (i.e., different values of τ_2 and τ_3), with small differences in packing caused by the differences in molecular geometry. The 20% tolerance on interatomic distances was chosen as sufficiently relaxed to

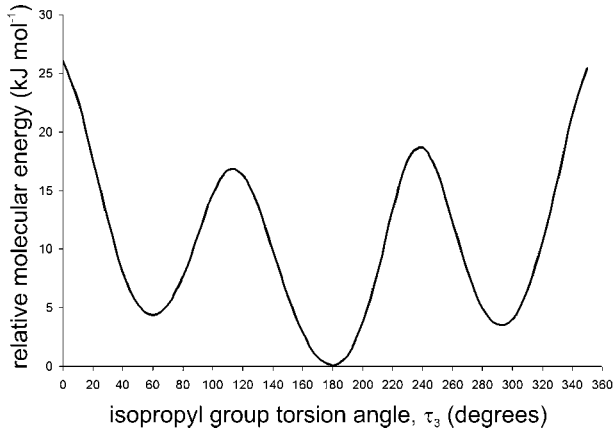

Figure 3. Conformational energy profile for rotation of the isopropyl group orientation τ_3 (with $\tau_1 = 180°$ and $\tau_2 = 0°$), calculated at the VWN/DNP level of theory (DMol3).

cluster such structures (*i.e.* treating them as identical) but not remove structures with distinct packing arrangements. The crystal structure with the lowest total energy from each cluster is retained, and, in this way, the version of each crystal structure with its most favorable conformation is retained and moved forward to the structural and energetic refinements in the latter steps.

Results and Discussion

A. Molecular Conformational Analysis. Conformations for the crystal structure searches were chosen using a similar approach to our previous study of alanine:[19] the amino group was kept fixed in the staggered conformation ($\tau_1 = 180°$), and conformations were taken with the carboxylate torsion angle (τ_2) incremented in 15° steps from 15° to 75°, a range chosen from an analysis of similar molecules in the CSD. 10° increments in τ_2 were used in our alanine calculations, but postanalysis found that a coarser sampling (20° steps) would have sampled conformational space sufficiently.[19] Here, we use the intermediate step size of 15°, which should generate as close to the full set of low energy crystal structures as possible while lowering the number of crystal structure generation calculations. Starting points for τ_3 were chosen from a DFT torsional energy scan of the isopropyl group (Figure 3), which showed three local minima, corresponding to staggered configurations of the β-carbon to α-carbon bond. The five orientations of the carboxylate group were combined with the three isopropyl group minimum energy orientations, giving fifteen conformations with which trial crystal structures were generated.

B. Generation of Crystal Structures. To check that the search located the known racemic valine polymorphs, the crystal structures generated with the rigid molecule conformations (Figure 1, step B) were compared with the true DL-valine crystal structures extracted from the CSD; good representations of both polymorphs were located with several of the molecular conformations (Table 1). However, the energetic rankings of the known structures among the predictions are poor, even among the separate lists from each molecular conformation, both in terms of the number of lower energy computer-generated crystal structures than the known structure, N_{lower}[4] (a perfect prediction would give $N_{lower} = 0$), and the energy difference between the known structure and the lowest energy computer-generated structure, ΔE (we are aiming for low values, with $\Delta E < 0$ if no unobserved computer-generated crystal structures have better calculated energies than the known polymorphs). For small rigid molecules, ΔE is usually less than 2−3 kJ mol^{-1} and N_{lower} is normally less than 5, when a high quality intermolecular model potential is used.[5]

Table 1. Rigid Conformations That Led to a Match to the Known Crystal Structures of DL-Valine

torsion angles			VALIDL ($P2_1/c$)		VALIDL02 ($P\bar{1}$)	
τ_1	τ_2	τ_3	N_{lower}[a]	ΔE[b]/kJ mol^{-1}	N_{lower}[a]	ΔE[b]/kJ mol^{-1}
180°	15°	60°	28	10.3	16	8.2
180°	30°	60°	26	7.8	16	6.5
180°	45°	60°	36	6.4	30	5.3
180°	60°	60°	105	13.9	88	11.9

[a] N_{lower} is the number of lower energy predicted crystal structures among the set of structures generated for that conformation. [b] ΔE is the energy difference between the computer-generated version of the observed crystal structure and the lowest energy predicted crystal structure for that molecular conformation.

These poor rankings can partly be attributed to the use of rigid molecular geometries when generating the trial crystal structures, as τ_3 in the observed DL-valine crystal structures ($\tau_3 \sim 80°$) is approximately 20° away from the closest minimum on the conformational energy surface (Figure 3). These results highlight a limitation of the method previously applied to the crystal structure prediction of alanine, in that the true crystal structures might be poorly ranked if the starting molecular geometries differ significantly from their optimum conformations in the crystal structures. The intermediate energy minimization step (Figure 1, step C) in which the molecular conformation can adjust to the crystal structure is included here to alleviate this problem.

C. Lattice Energy Minimization with Molecular Flexibility. The results using rigid molecular models fixed at the set of initial molecular geometries (Table 1) are clearly unsatisfactory, so all crystal structures were energy minimized again but without the rigid molecule constraints: the important torsion angles (τ_1, τ_2, τ_3, Figure 2) were given freedom to adjust to their crystal packing environments. We use force field descriptions of intramolecular degrees of freedom in this step and are mainly concerned with the force field's ability to provide a reliable description of the molecular structure in the crystal. Therefore, we tested a set of force fields by energy minimizing the known crystal structures of two molecules: L- and DL-alanine and leucine, the amino acids with a slightly smaller (alanine) and larger (leucine) hydrophobic side group than valine. We then compared a selection of torsion angles in the optimized crystal structures with those in the experimentally determined structures. Based on these tests (detailed results are deposited as Supporting Information), we chose the Dreiding force field as providing the best results. Therefore, we used the Dreiding force field for the flexible molecule energy minimization of the computer-generated crystal structures of valine.

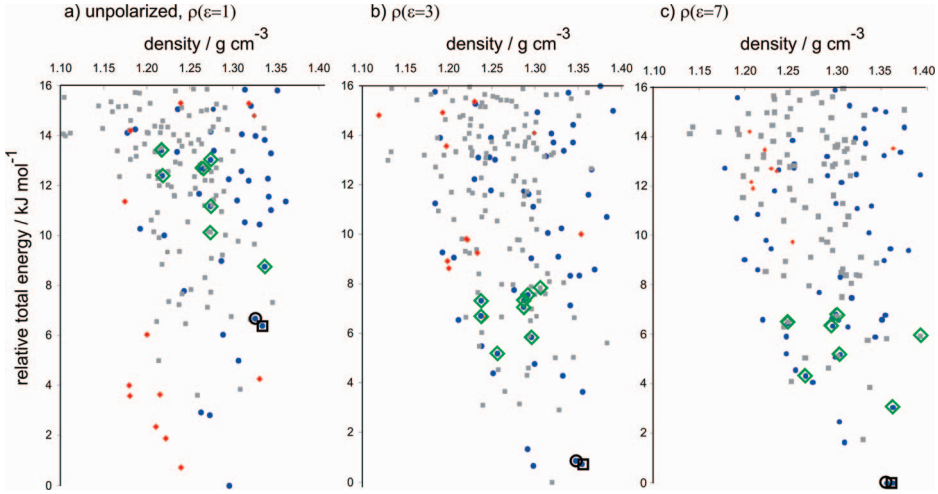

Figure 4. Plot of density vs relative energy for the computer-generated crystal structures of DL-valine after minimization with the Dreiding flexible force field followed by calculation of the total energies using the *exp-6* model potential, atomic multipoles, and DFT for the molecular energies. Electrostatic models and relative molecular energies were taken from a) the isolated molecule, b) PCM calculations with $\epsilon = 3$, and c) PCM calculations with $\epsilon = 7$. Structures are color coded by their lattice (intermolecular) energies: blue circles have intermolecular energies within 20 kJ mol^{-1} of the lowest lattice energy structure; gray squares have intermolecular energies between 20 and 40 kJ mol^{-1} above the lowest lattice energy structure; and red diamonds have intermolecular energies more than 40 kJ mol^{-1} above the lowest lattice energy structure. The known crystal structures of DL-valine are indicated by the open circle (monoclinic, CSD refcode VALIDL) and open square (triclinic, CSD refcode VALIDL02). Structures highlighted by open green diamonds show high structural similarities to the known crystal structures.

During this step, valine molecules in the computer-generated crystal structures were treated as comprising four rigid units; their relative orientations were allowed to relax at this stage while constraining the internal geometries of these rigid units at their DFT optimized geometries.

D. Refinement of the Lattice Energies. Clustering of the structures after energy minimization with the Dreiding force field resulted in 1130 distinct crystal structures. Each of these was then subjected to the final energy minimization step, where the molecular geometry was constrained at the geometry resulting from the Dreiding force field lattice energy minimization. The molecular geometry was extracted from *each* crystal structure, and a single point DFT molecular energy calculation was performed to obtain the molecular energy and electron density distribution. A distributed multipole analysis was performed on the resulting wave function, and then the crystal structure was lattice energy minimized using the *exp-6* + DMA model intermolecular potential. Total crystal energies were calculated as a sum of the atom-atom intermolecular energy and the DFT molecular energy.

We first examined the resulting set of crystal structures when the molecular properties (energy and atomic multipoles) were taken from isolated molecule DFT calculations. The results are summarized *via* a relative total energy vs density plot (Figure 4a), on which each point represents a distinct crystal structure. Furthermore, we color coded the points according to the intermolecular contribution to the total crystal energy.

Many of the crystal structures with lowest total energies using this model have poor *inter*molecular contributions to their energies (red diamonds in Figure 4a, which cover intermolecular energies in the range −172 to −152 kJ mol^{-1}). These crystal structures are clearly stabilized by favorable *intra*molecular energies, at the expense of strongly stabilizing *inter*molecular interactions. The computer-generated structures that correspond to the known polymorphs of DL-valine are ranked as the 15th (triclinic, VALIDL02) and 19th (monoclinic, VALIDL) lowest energy structures, 6.4 kJ mol^{-1} and 6.7 kJ mol^{-1} higher in energy than the computer-generated crystal structure with the lowest energy. While this is an improvement over the ranking with rigid molecular geometries (Table 1), the results are still unsatisfactory for crystal structure prediction, where we expect to find any observed crystal structures among the lowest energy structures. For rigid molecules, observed crystal structures are rarely outside of the 10 lowest energy structures and never more than about 5 kJ mol^{-1} above the lowest energy prediction.[5] Discounting the predicted crystal structures with very poor intermolecular packing energies (red diamonds in Figure 4a) improves the situation somewhat, but the known polymorphs remain farther from the global minimum than we would expect, suggesting inadequacies in the model we have used to evaluate the total relative energies.

The Influence of Molecular Polarization. We then explored the influence of including a polarizing environment when calculating the molecular energies and charge density distributions. The crystal structures were energy minimized using electrostatic models (distributed multipoles) derived from molecular wave functions calculated in a series of polarizing environments: the polarizable continuum model (PCM) with dielectric constants, ϵ, of 3 (typical for crystals of neutral organic molecules), 7 and 11 (chosen to represent the very polar environment in crystals with extreme charge separation). The effect of the continuum dielectric environment is to stabilize a greater charge separation in the molecule, influencing both the molecular energy and atomic

Table 2. Unit Cell Parameters and Relative Energies of the Observed and Predicted Crystal Structures of DL-Valine

	a/Å	b/Å	c/Å	α/°	β/°	γ/°	V_{mol}[a]/Å^3	ΔE[b]/kJ mol^{-1}
Monoclinic DL-Valine								
expt (room temperature, VALIDL)	5.21	22.10	5.41	90	109.2	90	294.2	-
predicted (unpolarized ρ)	5.259	22.185	5.284	90	107.9	90	293.4	+6.7
predicted, ρ(ϵ=3)	5.233	22.208	5.220	90	107.8	90	288.8	+0.9
predicted, ρ(ϵ=7)	5.225	22.219	5.195	90	107.9	90	287.0	0
predicted, ρ(ϵ=11)	5.222	22.223	5.187	90	107.9	90	286.3	0
Triclinic DL-Valine								
expt (120 K, VALIDL02)	5.222	5.406	10.838	90.9	92.3	110.0	287.1	-
predicted (unpolarized ρ)	5.252	5.287	11.139	89.7	82.4	107.9	291.5	+6.4
predicted, ρ(ϵ=3)	5.221	5.224	11.155	97.1	90.3	107.8	287.3	+0.7
predicted, ρ(ϵ=7)	5.194	5.214	11.473	100.1	90.4	107.8	290.8	+0.0
predicted, ρ(ϵ=11)	5.187	5.212	11.166	96.8	90.4	107.8	285.1	+0.1
L-Valine								
expt (120 K)	9.682	5.247	11.930	90	90.6	90	303.0	-
minimized[c] (unpolarized ρ)	9.787	5.228	11.735	90	90.5	90	300.3	−9.1
minimized,[c] ρ(ϵ=3)	9.666	5.195	11.752	90	90.5	90	295.0	−16.4
minimized,[c] ρ(ϵ=7)	9.613	5.182	11.760	90	90.5	90	292.9	−17.3
minimized,[c] ρ(ϵ=11)	9.595	5.178	11.764	90	90.5	90	292.3	−16.9

[a] V_{mol} is the crystal structure volume per molecule. [b] ΔE is the sum of the intermolecular lattice energy and the molecular energy (relative to the energy of the lowest energy conformation in any of the computer-generated crystal structures). [c] The result of energy minimization of the experimentally determined crystal structure using the same molecular model and procedure as used in the prediction calculations.

multipoles (the electrostatic model in the lattice energy calculation). The results, summarized as energy vs density plots for $\epsilon = 3$ and $\epsilon = 7$ in Figure 4b,c, show a strong dependence of the energetic ordering of the predicted crystal structures with the choice of ϵ. The crystal structures with poor intermolecular energies (red diamonds) are disfavored when the polarized molecular charge distributions are used, such that these structures are all outside of the lowest 8 kJ mol^{-1} range on total energy when using even a modestly polarized model ($\epsilon = 3$). As the computer-generated crystal structures with poor intermolecular energies are disfavored, those with the best intermolecular energies (blue circles, Figure 4) dominate the low energy region, and the ranking of the two known DL-valine polymorphs improves dramatically. The monoclinic (VALIDL) and triclinic (VALIDL02) polymorphs are the fourth and third lowest energy structures overall when using molecular energies and electrostatics derived with $\epsilon = 3$ and are first and second (i.e., the two lowest energy structures) with both $\epsilon = 7$ and $\epsilon = 11$. By calculating the molecular energies and charge density distributions in a polarizing environment, the ranking on total energy predicts the two known polymorphs perfectly, a dramatic improvement over results using unpolarized molecular models.

Table 2 summarizes structural information for the observed and predicted crystal structures of valine. Unit cell dimensions are in line with what should be expected. Cell dimensions and angles are all within 3% of the observed values, while the crystal structure volumes per molecule (V_{mol}) are all within 4%. There is a trend of compaction of the predicted structures with increased polarization (higher ϵ), because of the enhanced attractive interactions between polarized molecular charge densities. While the volumes of the predicted crystal structures minimized with multipoles calculated in a vacuum are close to the observed volumes, those using the polarized molecular models are contracted slightly. The change in volume with the polarized models is consistent with the expansion of amino acid structures from low temperature to room temperature[42] and the temperature-free (i.e., classical 0 K) nature of the predictions.

Analysis of the Components of the Total Energy. To determine the origin of the striking changes in the relative total crystal energies upon molecular polarization, the individual components of the total crystal energies (see eq 1) were further examined. The two energy contributions that are directly a function of the calculated electron density, ρ, are the DFT molecular energy and the calculated electrostatic component of the intermolecular energy; both include contributions from the induction energy when calculated from the polarized molecular charge densities. The variation of these two contributions with the value of ϵ used in the molecular PCM calculation is shown for the 20 lowest energy crystal structures (taken from the original set, Figure 4a) in Figure 5a,b. The isolated molecule calculations are included as $\epsilon = 1$.

The *absolute* values of the molecular energies in the 20 crystal structures increase by between 18.6 and 23.8 kJ mol^{-1} between isolated molecule calculations and PCM calculations with $\epsilon = 11$. However, the subsequent effect on the ranking of the crystal structures is small because the *relative* molecular energies among the conformations found in the low energy crystal structures only change by a few kJ mol^{-1}; the total range of molecular energies among these 20 crystal structures is 51 kJ mol^{-1} from the isolated molecule calculations and 55 kJ mol^{-1} in the most polarizing environment ($\epsilon = 11$), Figure 5a. This change in relative intramolecular energies has some influence on the final crystal structure ranking but is not the main cause of the important changes in total relative crystal energies when the polarized molecular models are used. The molecular energies in both observed DL-valine crystal structures, relative to the most stable conformations found in any of the predicted crystal structures, *increase* from about 46 kJ mol^{-1} (isolated molecules) to 51 kJ mol^{-1} (PCM, $\epsilon = 11$), i.e. they have gained no stability relative to the other putative crystal

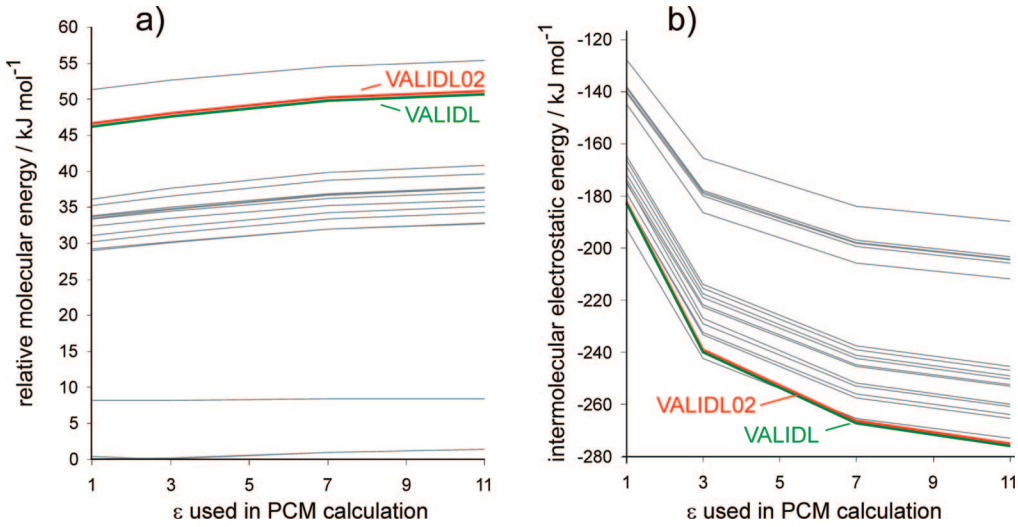

Figure 5. Variation in a) relative molecular energy (relative to the energy of the lowest energy conformation in any of the crystal structures) and b) intermolecular electrostatic energy as a function of the dielectric constant, ϵ, used in the molecular PCM calculation for the 20 lowest energy computer-generated crystal structures of DL-valine (from the $\rho(\epsilon=1)$ ranking).

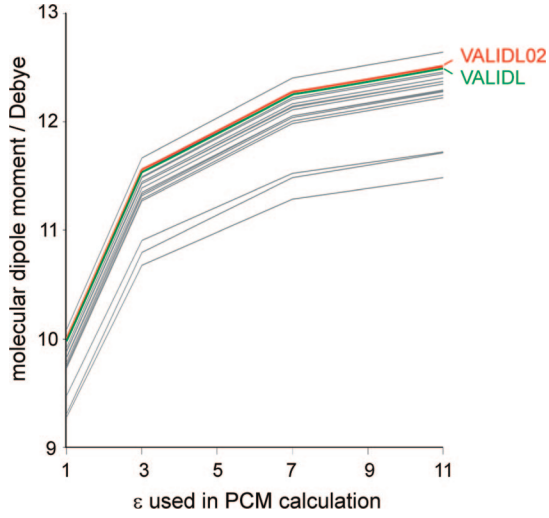

Figure 6. Variation in the molecular dipole moment as a function of the dielectric constant, ϵ, used in the molecular PCM calculation for the molecular geometries from the 20 lowest energy computer-generated crystal structures of DL-valine (from the $\rho(\epsilon=1)$ ranking).

structures in terms of intramolecular energy by accounting for the polarizing environment.

Electrostatic Energy. A much more pronounced effect is seen in the electrostatic contribution to the intermolecular energies in the crystal structures (Figure 5b). The cause of the large changes in calculated electrostatic energy is clear from the changes in molecular dipole moments between the vacuum calculations and those in a dielectric medium (Figure 6). The molecular dipole moments calculated for isolated molecules, which range from 9.3 to 10.1 Debye for the conformations in these 20 crystal structures, are far too low compared to the experimentally observed dipole moment from analysis of the X-ray determined charge density of triclinic DL-valine, which is 14.3(4) Debye.[43] The greatest change in dipole moments comes between the vacuum calculations and PCM ($\epsilon = 3$) calculations, where the molecular dipole enhancement ranges from 15.1 to 15.9% for the conformations in these 20 crystal structures. The total increase up to $\epsilon = 11$ ranges from 23.7 to 25.8%, which is in good agreement with the 23% dipole moment enhancement of valine estimated from X-ray determined charge density analysis.[8] The molecular electron densities from the PCM calculations are much closer to the real charge distribution in the crystal than those calculated for molecules in a vacuum.

The plot of calculated electrostatic energy vs dielectric constant (Figure 5b) shows why the two observed structures have improved in ranking so drastically from the model based on vacuum calculations ($\epsilon=1$) to those taking into account the strongly polarizing crystal environment. If we take $\epsilon=3$ to be a realistic description of the bulk crystalline environment, we can estimate the induction energy for each computer-generated crystal structure from eq 2, as $[U_{electrostatic}(\epsilon=3) - U_{electrostatic}(\text{vacuum}, \epsilon=1) + \Delta U_{molecular}(\epsilon=3 - \text{vacuum})]$, a quantity that varies from -30.1 to -47.8 kJ mol^{-1} among these 20 lowest energy crystal structures. This 17.7 kJ mol^{-1} variation in induction energy between crystal structures is more than double the entire range in total energies for this set of putative crystal structures and demonstrates why the induction energy should not be ignored in crystal structure prediction, especially for such polar molecules, where the electrostatics dominate the lattice energies. The induction energy is greatest in the two crystal structures corresponding to the known DL-valine polymorphs (Figure 5b), and this energy contribution moves these structures from being poorly ranked with the unpolarized model to being among the best few structures in the list of crystal structures with polarization taken into account.

L-Valine. Enantiopure L-valine crystallizes in only one known crystal structure, in the space group $P2_1$ with two molecules in the asymmetric unit; the two molecules differ in the orientation of the isopropyl group, having $\tau_3 = 77°$ and 180° in the two independent molecules. While we did not generate crystal structures with two independent molecules, we can compare the observed crystal structure with the predicted $Z`=1$ alternatives. To do this, the observed

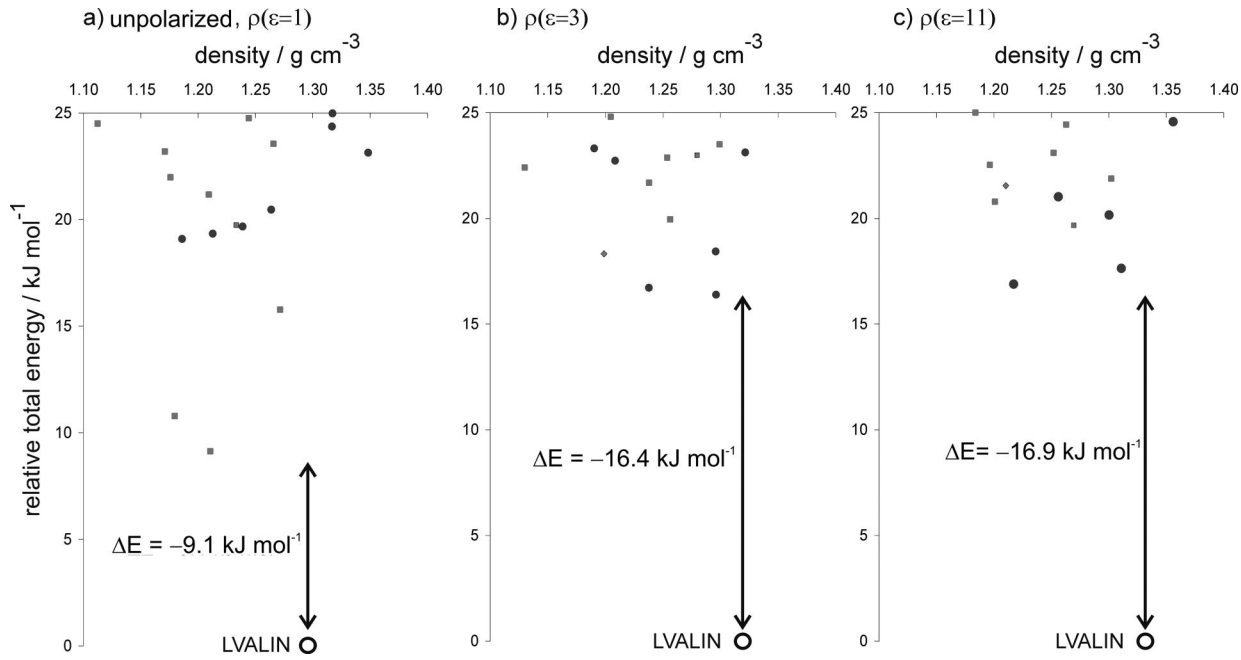

Figure 7. Plot of relative energy against density for the computer-generated $Z`=1$ crystal structures of L-valine after minimization with the Dreiding flexible force field and then calculation of the total energies using the *exp-6* model potential, atomic multipoles, and DFT for the molecular energies. Electrostatic models and relative molecular energies were taken from a) the isolated molecule, b) a PCM calculation with $\epsilon = 3$, and c) a PCM calculation with $\epsilon = 7$. The observed $Z`=2$ crystal structure of L-valine (LVALIN01) is indicated by an open circle, and the energy difference between it and the lowest energy predicted $Z`=1$ structure is indicated.

structure (CSD refcode LVALIN01) was energy minimized using the same method as the computer-generated crystal structures: bond lengths and bond angles were adjusted to those in the DFT molecular structure used for the crystal structure prediction calculations, and the structure was relaxed allowing flexibility of the torsion angles with the Dreiding force field, followed by a final rigid-molecule lattice energy minimization with the *exp-6* + DMA intermolecular model potential. The total energy was calculated as a sum of this intermolecular energy and the DFT molecular energy of the final molecular conformations. The final step was repeated with molecular calculations performed with and without the PCM polarizing environment.

With all models (based on vacuum and PCM molecular charge distributions) the observed $Z`=2$ crystal structure is considerably more stable than any of the putative $Z`=1$ structures (Figure 7). The total energy difference between the observed structure and lowest energy $Z`=1$ alternative is 9.1 kJ mol$^{-1}$ before including the effects of molecular polarization, and this gap increases to over 16 kJ mol$^{-1}$ when including the polarization of the molecules. The large difference between the observed structure and any of the predicted structures suggests that a $Z`=1$ polymorph of enantiopure valine is unlikely to ever be observed, at least within the space groups considered here.

In light of the results here, the success of our previous crystal structure prediction study of alanine[19] seems fortuitous. The results for alanine, where the true crystal structures (of both L-alanine and DL-alanine) were predicted without considering molecular polarization, do not demonstrate that the polarization contribution to the lattice energy is less important for that molecule but perhaps that the induction energy varies less among the possible low energy crystal structures of L- and DL-alanine than those of DL-valine. This may be a result of less variation in molecular conformations among the low energy crystal structures of alanine. We are currently studying a wider set of amino acid crystal structures to test the performance of our computational methods on a large set of similar molecules.

Conclusions

We have presented developments of our method for exploring the crystal packing landscape of flexible organic molecules, with the aim of crystal structure prediction. In this study, we have used computer-generated crystal structures of valine as a test of our approach and to evaluate a simple method for including the effects of polarization of the molecular charge density on the total relative energies of the known and putative polymorphs.

The results indicate that there is an imbalance in the intra- and intermolecular energy contributions to the total crystal energies if the molecular properties are taken from calculations on completely isolated molecules. To correct for this, molecular properties (energy and electron density distribution) have been calculated in a polarizing environment, described by the polarizable continuum model with dielectric constants chosen to be representative of molecular organic crystals (here, we tested values of ϵ ranging from 3 to 11). These calculations lead to molecular dipole moments that are more in line with X-ray charge density studies, and the changes in electrostatic and molecular energies give an estimate of the induction energy, which is very large for these crystal structures because valine crystallizes in zwitterionic

form. The PCM model contains no explicit information on the specific environment in each crystal structure, and the molecule in each crystal structure is immersed in the same structureless polarizing environment to polarize the molecular charge density. Therefore, the resulting polarization only distinguishes between crystal structures based on i) the conformational dependence of the molecular polarizability and ii) the different impact of molecular charge density polarization on intermolecular interactions in the various crystal structures. We view this as a first approximation to including induction energies in the assessment of relative stabilities of crystal structures, whereas a full treatment would need to model the specific, structured crystalline environment for each crystal structure.

Despite its apparent oversimplicity, the model leads to promising results here. The polarization favors those crystal structures with good intermolecular interactions over the other putative structures and, for both DL-valine and L-valine, preferentially stabilizes the true crystal structures over the many other low energy local minima. This leads to the two known polymorphs being ranked as the two lowest energy computer-generated crystal structures or as two of a small set of the lowest energy structures, depending on the value of ϵ when calculating molecular energies and charge distributions. The best choice of dielectric constant is uncertain, although the greatest effect on the molecular charge distribution is at low values and $2.5 \leq \epsilon \leq 4$ seems typical for crystals of neutral organic molecules.[44] Indeed, refractive index measurements[45,46] on L-amino acid crystal structures suggest values between about 2.25 and 2.5, which are slightly lower than static permittivities calculated by periodic DFT based lattice dynamics,[47] that suggest an average value of $\epsilon = 3.35$ for L-valine, with substantial anisotropy in the dielectric tensor. Empirically, we find that higher values of the dielectric constant perform better here: $\epsilon = 7$ results in a slightly better ranking of the known DL-valine crystal structures than $\epsilon = 3$, and higher values improve results even further. Higher dielectric constants also yield molecular dipole moments in better agreement with those from X-ray charge density studies. Our rationalization for these observations is that the higher values of ϵ might be compensating for the lack of specific interactions (such as hydrogen bonds) in the model; the calculations we use here introduce the polarizing effect of an average bulk environment but cannot model the strong polarizing effect of specific, directional intermolecular interactions. Side-by-side comparisons to polarization models that include the structure of the crystalline environment would be needed to investigate this further.

The results indicate that the effects of polarization in molecular crystals, which are usually ignored when modeling their structures and properties, can have a significant influence in calculations aimed at predicting the likely crystal structures of polar molecules. The method we have presented for including polarization in the calculations is computationally inexpensive and is being further tested and extended to the crystal structure prediction of more complex systems, in particular those of pharmaceutical interest such as more flexible molecules and multicomponent crystals (salts, cocrystals, and solvates).

Acknowledgment. We thank the Pfizer Institute for Pharmaceutical Materials Science for funding and Dr. Neil Feeder for helpful discussions. G.M.D. thanks the Royal Society for a University Research Fellowship.

Supporting Information Available: Structure files (CIF) of the 20 lowest energy predicted crystal structures of DL-valine with each of the four intermolecular electrostatic models (unpolarized molecules, $\epsilon = 3$, $\epsilon = 7$, and $\epsilon = 11$), structure files (CIF) of the 10 lowest energy predicted crystal structures of L-valine with each of the four intermolecular electrostatic models (unpolarized molecules, $\epsilon = 3$, $\epsilon = 7$, and $\epsilon = 11$), and tables summarizing the results of the testing of flexible molecule force fields for the crystal structures of alanine and leucine. This material is available free of charge via the Internet at http://pubs.acs.org.

References

(1) Chemburkar, S. R.; Bauer, J.; Deming, K.; Spiwek, H.; Patel, K.; Morris, J.; Henry, R.; Spanton, S.; Dziki, W.; Porter, W.; Quick, J.; Bauer, P.; Donaubauer, J.; Narayanan, B. A.; Soldani, M.; Riley, D.; McFarland, K. *Org. Process Res. Dev.* **2000**, *4*, 413–417.

(2) Morissette, S. L.; Almarsson, Ö.; Peterson, M. L.; Remenar, J. F.; Read, M. J.; Lemmo, A. V.; Ellis, S.; Cima, M. J.; Gardner, C. R. *Adv. Drug Delivery Rev.* **2004**, *56*, 275–300.

(3) Day, G. M.; Motherwell, W. D. S.; Ammon, H. L.; Boerrigter, S. X. M.; Della Valle, R. G.; Venuti, E.; Dzyabchenko, A.; Dunitz, J. D.; Schweizer, B.; van Eijck, B. P.; Erk, P.; Facelli, J. C.; Bazterra, V. E.; Ferraro, M. B.; Hofmann, D. W. M.; Leusen, F. J. J.; Liang, C.; Pantelides, C. C.; Karamertzanis, P. G.; Price, S. L.; Lewis, T. C.; Nowell, H.; Torrisi, A.; Scheraga, H. A.; Arnautova, Y. A.; Schmidt, M. U.; Verwer, P. *Acta Crystallogr. B* **2005**, *61*, 511–527.

(4) Day, G. M.; Chisholm, J.; Shan, N.; Motherwell, W. D. S.; Jones, W. *Cryst. Growth Des.* **2004**, *4*, 1327–1340.

(5) Day, G. M.; Motherwell, W. D. S.; Jones, W. *Cryst. Growth Des.* **2005**, *5*, 1023–1033.

(6) Görbitz, C. H. *J. Mol. Struct.-THEOCHEM* **2006**, *775*, 9–17.

(7) Allen, F. H. *Acta Crystallogr. B* **2002**, *58*, 380–388.

(8) Spackman, M. A.; Munshi, P.; Dittrich, B. *ChemPhysChem* **2007**, *8*, 2051–2063.

(9) Banks, J. L.; Kaminski, G. A.; Zhou, R. H.; Mainz, D. T.; Berne, B. J.; Friesner, R. A. *J. Chem. Phys.* **1999**, *110*, 741–754.

(10) Patel, S.; Brooks, C. L., III *J. Comput. Chem.* **2004**, *25*, 1–15.

(11) Applequist, J. *J. Chem. Phys.* **1985**, *83*, 809–826.

(12) Stone, A. J. *Chem. Phys. Lett.* **1989**, *155*, 102–110.

(13) Misquitta, A. J.; Stone, A. J.; Price, S. L. *J. Chem. Theory Comput.* **2008**, *4*, 19–32.

(14) Misquitta, A. J.; Stone, A. J. *J. Chem. Theory Comput.* **2008**, *4*, 7–18.

(15) Welch, G. W. A.; Karamertzanis, P. G.; Misquitta, A. J.; Stone,

A. J.; Price, S. L. *J. Chem. Theory Comput.* **2008**, *4*, 522–532.

(16) Cossi, M.; Barone, V.; Mennucci, B.; Tomasi, J. *Chem. Phys. Lett.* **1998**, *286*, 253.

(17) Mennucci, B.; Tomasi, J. *J. Chem. Phys.* **1997**, *106*, 5151.

(18) Cossi, M.; Scalmani, G.; Rega, N.; Barone, V. *J. Chem. Phys.* **2002**, *117*, 43–45.

(19) Cooper, T. G.; Jones, W.; Motherwell, W. D. S.; Day, G. M. *CrystEngComm* **2007**, *9*, 595–602.

(20) Mallikarjunan, M.; Rao, S. T. *Acta Crystallogr. B* **1969**, *25*, 296.

(21) Dalhus, B.; Görbitz, C. H. *Acta Crystallogr. C* **1996**, *52*, 1759.

(22) Dalhus, B.; Görbitz, C. H. *Acta Chem. Scand.* **1996**, *50*, 544.

(23) Day, G. M.; Motherwell, W. D. S.; Jones, W. *Phys. Chem. Chem. Phys.* **2007**, *9*, 1693–1704.

(24) Delley, B. *J. Chem. Phys.* **1990**, *92*, 508–517.

(25) *MS Modelling*, *release 3.0.1*; Accelrys Inc.: San Diego, U.S.A., 2004.

(26) Karamertzanis, P. G.; Pantelides, C. C. *J. Comput. Chem.* **2004**, *26*, 304–324.

(27) Cambridge Structural. Database - Space Group Statistics Web page. http://www.ccdc.cam.ac.uk/products/csd/statistics/space_group_stats.php4 (accessed January 3, 2008).

(28) Williams, D. E.; Cox, S. R. *Acta Crystallogr. B* **1984**, *40*, 404–417.

(29) Cox, S. R.; Hsu, L.-Y.; Williams, D. E. *Acta Crystallogr. A* **1981**, *37*, 293–301.

(30) Coombes, D. S.; Price, S. L.; Willock, D. J.; Leslie, M. *J. Phys. Chem.* **1996**, *100*, 7352–7360.

(31) Frisch, M. J.; Trucks, G. W.; Schlegel, H. B.; Scuseria, G. E.; Robb, M. A.; Cheeseman, J. R.; Montgomery, J. A.; Vreven, T.; Kudin, K. N.; Burant, J. C.; Millam, J. M.; Iyengar, S. S.; Tomasi, J.; Barone, V.; Mennucci, B.; Cossi, M.; Scalmani, G.; Rega, N.; Petersson, G. A.; Nakatsuji, H.; Hada, M.; Ehara, M.; Toyota, K.; Fukuda, R.; Hasegawa, J.; Ishida, M.; Nakajima, T.; Honda, Y.; Kitar, O.; Nakai, H.; Klene, M.; Li, X.; Knox, J. W.; Hratchian, H. P.; Cross, J. B.; Adamo, C.; Jaramillo, J.; Gomperts, R.; Stratmann, R. E.; Yazyev, O.; Austin, A. J.; Cammi, R.; Pomelli, C.; Ochterski, J.; Ayalla, P. Y.; Morokuma, K.; Voth, G. A.; Salvador, P.; Dannenberg, J. J.; Zakrzewski, V. G.; Dapprich, S.; Daniels, A. D.; Strain, M. C.; Farkas, O.; Malick, D. K.; Rabuck, A. D.; Raghavachari, K.; Foresman, J. B.; Ortiz, J. V.; Cui, Q.; Baboul, A. G.; Clifford, S.; Cioslowski, J.; Stefanov, B. B.; Liu, G.; Liashenko, A.; Piskorz, P.; Komaromi, I.; Martin, R. L.; Fox, D. J.; Keith, T.; Al-Laham, M. A.; Peng, C. Y.; Nanayakkara, A.; Challacombe, M.; Gill, P. M. W.; Johnson, B.; Chen, W.; Wong, M. W.; Gonzalez, C.; Pople, J. A. *Gaussian03*; Gaussian Inc.: Wallingford, CT, 2004.

(32) Stone, A. J. GDMA: Distributed Multipole Analysis of Gaussian Wavefunctions, version 2.2.; University of Cambridge: 2005.

(33) Stone, A. J. *Chem. Phys. Lett.* **1981**, *83*, 233–239.

(34) Stone, A. J.; Alderton, M. *Mol. Phys.* **1985**, *56*, 1047–1064.

(35) Price, S. L.; Willock, D. J.; Leslie, M.; Day, G. M. DMAREL, version 4.1.1; 2001.

(36) Dauber-Osguthorpe, P.; Roberts, V. A.; Osguthrope, D. J.; Wolff, J.; Genest, M.; Hagler, A. T. *Proteins* **1988**, *4*, 31–47.

(37) Sun, H. *J. Phys. Chem.* **1998**, *102*, 7338.

(38) Mayo, S. L.; Olafson, B. D.; Goddard, W. A. *J. Phys. Chem.* **1990**, *94*, 8897–8909.

(39) Rappe, A. K.; Casewit, C. J.; Colwell, K. S.; Goddard, W. A.; Skiff, W. M. *J. Am. Chem. Soc.* **1992**, *114*, 10024–10035.

(40) Gasteiger, J.; Marsili, M. *Tetrahedron* **1980**, *36*, 3219.

(41) Chisholm, J.; Motherwell, S. *J. Appl. Crystallogr.* **2005**, *38*, 228–231.

(42) Kozhin, V. *Kristallografiya* **1978**, *23*, 1211–1215.

(43) Flaig, R. Ph.D. Thesis, Freie Universität Berlin, Berlin, 2000.

(44) *Handbook of Chemistry and Physics*, 72nd ed.; CRC Press: Boston, MA, 1992; pp 12−38.

(45) Misoguti, L.; Varela, A. T.; Nunes, F. D.; Bagnato, V. S.; Melo, F. E. A.; Mendes Filho, J.; Zilio, S. C. *Opt. Mater.* **1996**, *6*, 147–152.

(46) Rodrigues Jr., J. J.; Misoguti, L.; Nunes, F. D.; Mendonça, C. R.; Zilio, S. C. *Opt. Mater* **2003**, *22*, 235–240.

(47) Tulip, P. R.; Clark, S. J. *Phys. Rev. B* **2006**, *74*, 064301.

CT800195G